A fly-locust based neuronal control system applied to an unmanned aerial vehicle: the invertebrate neuronal principles for course stabilization, altitude control and collision avoidance

Sergi Bermudez i Badia, Pawel Pyk and Paul F.M.J. Verschure

The International Journal of Robotics Research 2007; 26; 759
DOI: 10.1177/0278364907080253

Sergi Bermúdez i Badia

Laboratory for Synthetic Perceptive, Emotive and Cognitive Systems, Universitat Pompeu Fabra, Ocata num. 1, 08003 Barcelona, Spain
Institute of Neuroinformatics, ETH/University of Zurich
Winterthurerstr. 190, CH-8057 Zurich, Switzerland
sergi.bermudez@upf.edu

Pawel Pyk

Institute of Neuroinformatics, ETH/University of Zurich
Winterthurerstr. 190, CH-8057 Zurich, Switzerland

Paul F.M.J. Verschure

Laboratory for Synthetic Perceptive, Emotive and Cognitive Systems, Universitat Pompeu Fabra, Ocata num. 1, 08003 Barcelona, Spain
ICREA & Technology Department, University Pompeu Fabra
Passeig de Circumval.lació 8, 08003, Barcelona, Spain

A fly-locust based neuronal control system applied to an unmanned aerial vehicle: the invertebrate neuronal principles for course stabilization, altitude control and collision avoidance

Abstract

The most versatile and robust flying machines are still those produced by nature through evolution. The solutions to the 6 DOF control problem faced by these machines are implemented in extremely small neuronal structures comprising thousands of neurons. Hence, the biological principles of flight control are not only very effective but also efficient in terms of their implementation. An important question is to what extent these principles can be generalized to man-made flying platforms. Here, this question is investigated in relation to the computational and behavioral principles of the opto-motor system of the fly and locust. The aim is to provide a control infrastructure based only on biologically plausible and realistic neuronal models of the insect opto-motor system. It is shown that relying solely on vision, biologically constrained neuronal models of the fly visual system suffice for course stabilization and altitude control of a blimp-based UAV. Moreover, the system is augmented with a collision avoidance model based on the Lobula Giant Movement Detector neuron of the Locust. It is shown that the biologically constrained course stabilization model is highly robust and that the combined model is able to perform autonomous indoor flight.

The International Journal of Robotics Research
Vol. 26, No. 7, July 2007, pp. 759–772
DOI: 10.1177/0278364907080253

Figures 1–4, 6–13 appear in color online: http://ijr.sagepub.com

KEY WORDS—biologically based, insect vision, optic flow, neural model, LGMD, EMD, UAV, autonomous flight, blimp-based, altitude control, course stabilization, Reichardt correlation

1. Introduction

Nature has produced highly versatile and robust flying machines (Dudley 2000). Indeed it was bird flight itself that inspired the Wright brothers in the construction of the first fixed-wing air plane (Kelly 1950). In addition to having informed the construction of flying platforms themselves, nature can also provide us with solutions to the 6 DOF control problem faced by flying machines (Dudley 2000). For instance, dragonflies can fly in cluttered environments at a speed of 10^2 body lengths/s (Marden 2005), while a blowfly can make rapid flight maneuvers at up to 1.2 m/s, with accelerations of up to 20 m/s^2 (Schilstra and van Hateren 1999). These flight maneuvers are mainly generated by the opto-motor system of a brain of about 1 mm^3 comprising about 200,000 neurons (Posey et al. 2001). Although it is not the only system used for navigation, approximately two-thirds of the fly brain is dedicated to visual processing (Strausfeld 1976). Hence, the brain of flying insects includes principles of visual flight control that are not only very effective but also efficient in terms of their implementation. An important question is to what extend these principles can be generalized to man-made flying platforms. Here we investigate this question in relation to the computational

and behavioral principles of the opto-motor system of the fly and locust. We will evaluate to what extend a biologically constrained neuronal model of this system is able to control an Unmanned Aerial Vehicle (UAV).

A large number of models for insect based opto-motor behavior have been proposed and many of these show reasonably good results (Harrison 2005; Netter and Franceschini 2002; Martin and Franceschini 1994; Franceschini et al. 1992). However, occasionally biologically unrealistic sensors are included in the control system to achieve a functional result (Zufferey et al. 2002; Ichikawa et al. 2001). Instead, as opposed to resorting to additional sensors we aim at providing a control infrastructure based only on vision and biologically plausible and realistic neuronal models of the insect opto-motor system. In addition, a considerable amount of work has been done on obstacle avoidance, homing and trajectory following using ground based robots (Netter and Franceschini 2002; Harrison 2005; Blanchard and Verschure 1999; Blanchard et al. 2001; Hafner et al. 2002; Hafner and Salomon 2002; Martin and Franceschini 1994; Franceschini et al. 1992). However, despite the relevance of these robot experiments, using ground based mobile robots as a platform reduces the 6 DOF problem that flying insects need to solve to a 3 DOF problem. The latter negotiate complex dynamics that include inertia and 6 DOF that lead to problems of course stabilization, altitude and position control that ground based systems do not have to face. Hence, we will use flying robots to investigate and reconstruct the principles underlying biological flight control systems. The insect flight control system is of particular interest because of its ability to show robust flight stabilization, collision avoidance, secure takeoff, landing and so on using relatively simple visual mechanisms (Tammero and Dickinson 2002; Srinivasan et al. 1996; Egelhaaf and Borst 1993; Egelhaaf 1985; Reichardt 1961). In the field many types of UAVs are and have been used, most of these helicopter, fixed wing or blimp based (Skafidas 2002; Iida 2001; Zufferey et al. 2002; Musial et al. 2000; Saripalli et al. 2003; Netter and Franceschini 2002). Since our opto-motor model is a component of a larger system that has to serve chemical localization and search (Pyk et al. 2006) we limit its application to a dirigible that will exert a minimal effect on the structure of the chemical plumes in its environment.

2. Methods and Materials

2.1. Setup

We have developed a blimp-based robot designed to work within indoor environments (Figure 1). The dimensions of the hull are 30 by 120 cm (radius × length) that provides for a payload of about 250 g at 600 m over sea level. Four propellers are mounted in a lightweight balsa wood structure providing the robot with independent control for altitude and translation. The propellers (DIDEL SA, Belmont, Switzerland, www.didel.com) are hand made and optimized for the combination of motors (08GS – 8 mm motor, API-Portescap, La Chaux-de-Fonds, Switzerland, www.portescap.com) and 1:7 gearboxes (8R78 mm, DIDEL SA, Belmont, Switzerland, www.didel.com), providing 20 g thrust per motor at full speed. The robot is powered using a 10 g lithium-polymer battery (West-technik, Germany) providing for about one hour of autonomous flight.

The UAV is equipped with two CCD color cameras ("Module 3", Conrad Electronics, Germany) mounted on the front part separated by 110°, pointing to the left and right side respectively. Each of these lightweight high-resolution cameras (628 [H] x 582 [V] pixels) is equipped with a wide-angle lens (2.5 mm lenses, Conrad Electronics, Switzerland). Given the opening angle of the cameras (100 [H] × 87 [V] degrees), the combined camera system covers over 180° of the frontal horizontal sphere. The images acquired with the cameras are transmitted via two lightweight PAL transmitters (SDX-21LP video transmitters working in the 2.4 GHz band, produced by RF-Video, Canada) to our ground station where they are further processed. An on-board radio receiver allows the remote control of the speed of all the motors independently via a radio link. Serial communication with the flying platform is established using a pair of BIM433-F transceivers (Wireless World AG, Switzerland), allowing for up to 115200 baud. The ground station setup consists of two PAL receivers (Wavecom, RF-Video, Canada) that receive the signals from the on board cameras; a quad combiner (Grand Virtual Guard, ARP Datacon) that combines them together in just one image; and a USB frame grabber (Lifeview USB Capview, Lifeview, Taiwan) that allows a laptop or PC to acquire the video stream.

2.2. Experimental Room and 3D Tracking System

Experiments are performed in a 5 × 4 × 4.5 m room with randomly distributed solid black squares on the walls and the floor as visual cues (Figure 1). In order to analyze and quantify the trajectory and the behavior of the UAV accurately, we have developed a 3D real time visual tracking system that provides us with the position (x, y, z), heading direction (x_h, y_h, z_h) and linear velocity of the UAV. The tracking system, uses two infrared cameras (2.5 mm lenses, Conrad Electronics, Switzerland) mounted at the ceiling at 4.5 m and uses stereoscopy to infer the 3D position of two IR LEDs mounted on top of the hull of the UAV. The transformation of the two camera pixel coordinates into a pair of three dimensional positions is achieved with a multilayer perceptron. A large number of regular spaced pre-mapped positions in the room are used as reference points for interpolation. The tracking system achieves an accuracy of up to 5 cm. Furthermore, the tracking data is acquired synchronously with the internal states and responses of the neural model that controls the flight behavior. Hence, we

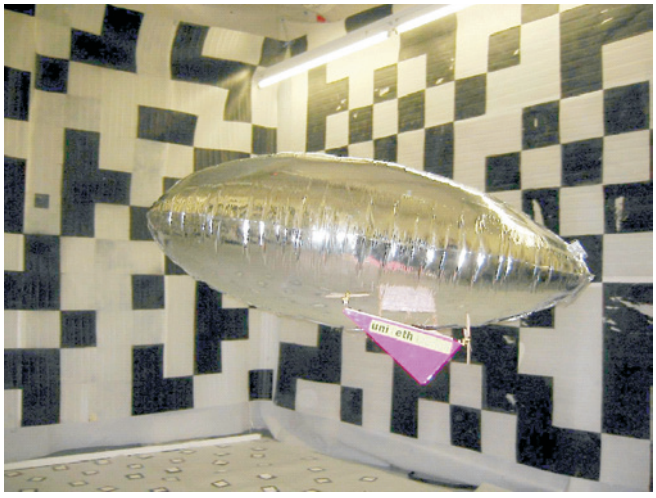

Fig. 1. Image of the blimp-based UAV in our test arena. The walls and the floor of the 5 × 4 × 4.5 m room are covered with randomly distributed black squares to provide visual cues to the UAV. A vision based tracking system is mounted at the ceiling of the room, providing us with the position, orientation and velocity of the UAV.

are able to directly correlate the neuronal states of our model to the behaviors produced by the UAV. The data acquisition is performed at 5 Hz and the data analysis is performed using Matlab (Mathworks, USA) and our simulation environment IQR421 (Bernardet et al. 2002).

3. Models

Our neuronal model includes components for course stabilization, altitude control and collision avoidance and is derived from our current understanding of the insect opto-motor system (Reichardt 1961; Egelhaaf and Borst 1993; Srinivasan et al. 1996; Kern et al. 2001; Braitenberg 1967). Our model comprises several processes performed in different layers of the insect visual system (Figure 2). These systems are considered to have a hierarchical organization where the signals from the photoreceptors are ultimately integrated in the response of, so called, wide field neurons that are tuned to specific properties of the visual input. For this reason these high-level neurons are also called matched filters. The first step in the processing hierarchy occurs at the level of the lamina where the luminance signal acquired by the photoreceptors is normalized using a logarithmic compression (Levine 1985) with:

$$I_{photo} = k_i \cdot \log(k_j I_{input} + const) \tag{1}$$

where I_{photo} is the photoreceptor response, I_{input} the input luminance level and $k_i, k_j, const$ scaling constants. Subsequently an edge enhancement is performed in the Lamina using a centre/surround inhibition, a method similar to a difference of Gaussians based zero-crossing edge extraction (Gonzalez and Woods 1992):

$$Edge_{image} = Input_{image} * DiffGauss_{Kernel} \tag{2}$$

where $Input_{image}$ is an input image, $DiffGauss_{Kernel}$ a difference of Gaussians kernel and $Edge_{image}$ the resulting image from the convolution operation.

$$DiffGauss_{Kernel} = f(\mu, \sigma_1) - f(\mu, \sigma_2) \tag{3}$$

$$f(\mu, \sigma) = \frac{1}{\sqrt{2\pi}\sigma} \exp\left(\frac{-(x+\mu)^2}{2\sigma^2}\right) \tag{4}$$

with μ the mean value, and $\sigma_1 > \sigma_2$ fixed standard deviation values.

After the isolation of the contrast information, three parallel processing streams deal with extracting optic flow information relevant for flight stabilization, altitude control and collision avoidance. There are two different priority levels: stabilization and altitude control responses are inhibited whenever a collision is detected, hence, an avoidance action is always prioritized.

3.1. Course Stabilization and Altitude Control: Elementary Motion Detectors and the HS/VS system

Course stabilization and altitude control are achieved by reacting to any drift or perturbation of basic optic flow patterns (Srinivasan et al. 1996). These optic flow patterns are detected by the, so called, wide-field Horizontal and Vertical System neurons (HS and VS respectively) located in the Lobula plate layer (Hengstenberg 1982). These cells are known to be motion sensitive and they respond maximally to a stimulus moving in a certain preferred direction whereas they show a decrease in the membrane potential due to stimuli moving in the opposite direction, i.e. null direction (Egelhaaf and Borst 1993; Egelhaaf 1985). The responses of these visual neurons result from the integration of the activity of local visual motion sensitive cells called Elementary Motion Detectors (EMDs). Since these neurons are able to extract egocentric motion information, they are therefore good candidates to be used for a set of tasks such as course stabilization, altitude control, odometry, etc. (Srinivasan et al. 1996; Tammero and Dickinson 2002; Franceschini et al. 1992). Both HS and VS cells are neurons of the visual system believed to be involved in providing relevant visual information that is used in flight control (Egelhaaf 1985). These cells encode the direction of rotation of the animal largely independent of the spatial layout and texture of the environment (Hengstenberg 1982). Only when the animal is very close to an object are the responses affected (Kern et al. 2001; Tammero and Dickinson 2002).

In the specific case of *Drosophila,* there are about 800 ommatidia and 8 photoreceptors (R1–R8) per ommatidia (Ready

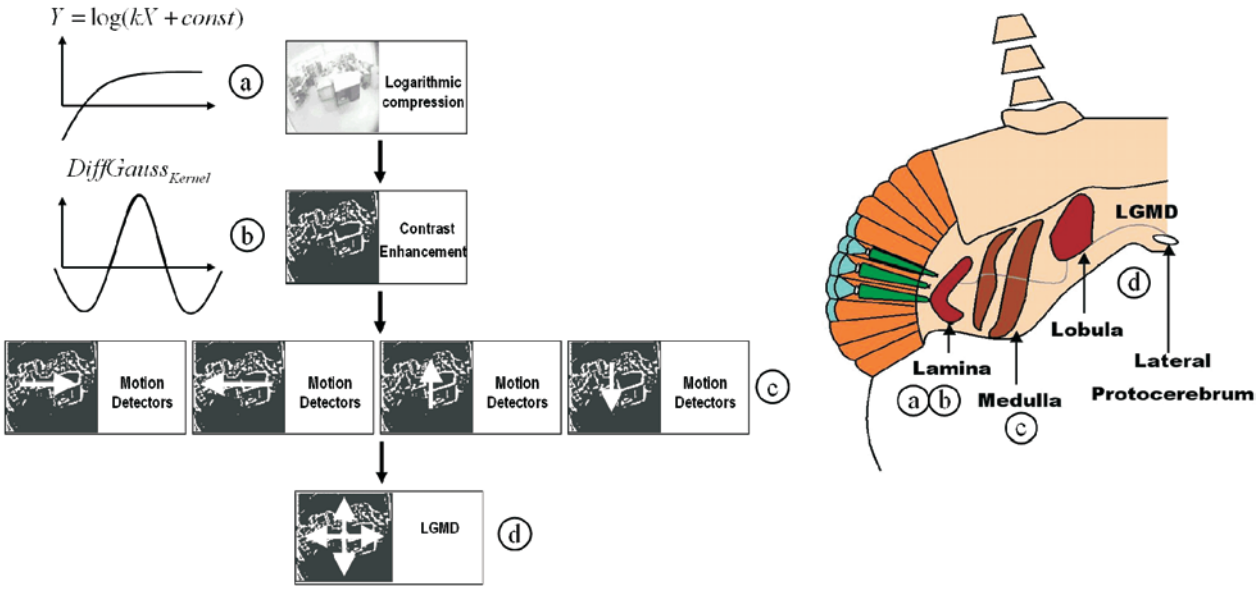

Fig. 2. Functional (left) and anatomical (right) structure of a prototypical insect visual system based on the locust. See text for further explanation.

et al. 1976). In our implementation a slightly lower resolution is used instead: 25 × 25 input pixels (625 pixels). Furthermore, flies have about 50–60 wide-field motion sensitive neurons or tangential cells that encode motion information (Hengstenberg 1982). Instead, our implementation only makes use of four wide-field motion sensitive neurons. In our model, these cells integrate the response of 25 × 25 local motion sensitive cells (EMDs). A higher resolution is impractical since the computational cost would slow down the system and would provoke aliasing related problems. In contrast, a lower resolution would reduce the motion sensitivity of the model. Since, each one of the EMDs is sensitive only to local motion in the visual field (Egelhaaf and Borst 1993; Egelhaaf 1985; Douglas and Strausfeld 1996; Reichardt 1961), the integration of the EMDs over the whole visual field produces a VS/HS cell type of response that encodes the ego-motion of the insect. Using this information provided by the HS/VS cells we can generate the motor actions that will compensate for any drift of the UAV or maintain a specific altitude.

Up to now we have described a hierarchical structure that goes from the photoreceptors to the selection of the opto-motor action. Every layer described above performs an important operation that only makes sense in the given context of the neural structure. Therefore, the output of the HS/VS cells can only be understood as the integration of EMDs, and those in turn only as a pairwise processing of neuronal responses in the Lamina and so on.

The so called "correlation model" of the EMDs, or Reichardt correlator, was proposed long ago (Reichardt 1961) and this model only requires a few elaborations to reflect the specific physiological features of the fly's motion detection system (Egelhaaf and Borst 1993; Higgins et al. 2004) (Figure 3).

The Reichardt correlation model is applied at the pixel level between neighboring pixels (I_a and I_b in Figure 3) separated by a certain distance D. There are two branches, the null and preferred output, which are computed independently. Given a translating object from pixel a to b at speed v, the Reichardt correlation $Rcorr(I_a, I_b)$ is defined as:

$$\begin{aligned} Rcorr(I_a, I_b) &= Out_{preferred}(I_a, I_b) \\ &- Out_{null}(I_a, I_b) \end{aligned} \tag{5}$$

$$Out_{preferred}(I_a, I_b) = I_a(t-\delta) \cdot I_b(t) \tag{6}$$

$$Out_{null}(I_a, I_b) = I_b(t-\delta) \cdot I_a(t). \tag{7}$$

Given the speed v and a pixel separation of D,

$$I_b(t) = I_a(t - D/v) \tag{8}$$

then,

$$\begin{aligned} &Out_{preferred}(I_a, I_a(t - D/v)) \\ &= I_a(t-\delta) \cdot I_a(t - D/v). \end{aligned} \tag{9}$$

We find that $Out_{preferred}$ and Out_{null} are maximum when,

$$\frac{\partial}{\partial \delta} Out_{preferred} = 0, \quad \text{for} \quad \delta = D/v \tag{10}$$

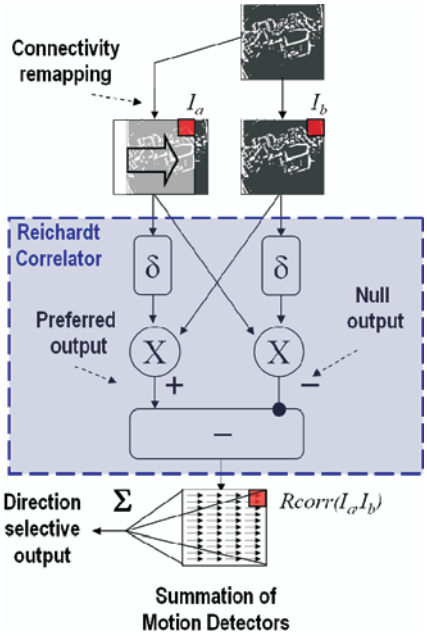

Fig. 3. HS/VS cell implementation, making use of the Reichardt correlation (Reichardt 1961), where δ represents a delay, X multiplication and – subtraction. In this case, the preferred direction of motion is rightward (arrow). The Reichardt correlation ($Rcorr(I_a, I_b)$) is extracted between neighboring pixels (I_a, I_b). The result of all pixel level correlations is spatially integrated to construct a wide field directionally selective output.

and

$$\frac{\partial}{\partial \delta} Out_{null} = 0, \quad \text{for} \quad \delta = -D/v. \tag{11}$$

The resulting wide field motion selective output is:

$$\begin{aligned} Output_{directional} &= \sum_{i}^{pixels} Rcorr\left(I_i, I_i(t - D/v)\right) \\ &= \sum_{i}^{pixels} Out_{preferred}\left(I_i, I_i(t - D/v)\right) \\ &- Out_{null}\left(I_i, I_i(t - D/v)\right) \end{aligned} \tag{12}$$

and given $I_j = I_i(t - D/v)$,

$$\begin{aligned} Output_{directional} &= \sum_{i,j}^{pixels} Out_{preferred}\left(I_i, I_j\right) \\ &- Out_{null}\left(I_i, I_j\right). \end{aligned} \tag{13}$$

We observe that the Reichardt detector is optimized for a certain speed. The closer D/v is to δ, the higher the preferred output is (equation (10)); and therefore, the closer D/v is to $-\delta$, the higher the null output is (equation (11)). The subtraction of the null branch to the preferred one results in a local motion directional selective response.

The integration of the EMD responses with the same preferred direction over the whole visual field encodes the total motion perceived in that particular direction and provides a HS/VS type of response (equation (13)). After computing the response difference of left and right, and up and down motion sensitive neurons, a winner-take-all network decides the actual direction of motion and intensity for both altitude and translation, and consequently the appropriate compensation motor command. The neural action states are read-out by the neural simulator software iqr421 and packaged into a motor command that is transmitted to the UAV.

3.2. Collision Avoidance: The Lobula Giant Movement Detector

The target animal to be studied for the neuronal correlate of obstacle avoidance in the insect brain is the locust. This insect is known to have a highly specialized neuron in the Lobula plate that responds to imminent collisions or approaching predators: the Lobula Giant Movement Detector (LGMD). Many studies have focused on this neuron and a number of neural models have been proposed. As opposed to the course stabilization task, a few biologically plausible models for collision avoidance have been proposed and applied to mobile robots (Blanchard and Verschure 1999; Blanchard et al. 2001; Harrison 2005). So far, however, none of these have been tested on UAVs (Iida 2001; Zufferey et al. 2002, Netter and Franceschini 2002).

The LGMD increases its firing rate in response to an approaching object. Recent studies have modeled the LGMD responses using a multiplication operation between the angular velocity θ', and angular size θ, of an approaching object:

$$\begin{aligned} F &= \theta' \exp\left(-\alpha \cdot \theta\right), \\ \text{with} \quad \alpha &= \frac{1}{\tan\left(\theta_{threshold}/2\right)}. \end{aligned} \tag{14}$$

Here F represents the output firing rate and $\theta_{threshold}$ is an animal and species dependent parameter. It has been shown that equation (14) provides a very accurate description of the responses of the LGMD neuron to looking stimuli (Gabbiani et al. 2002). Hence, we will use it as a benchmark for our own model of this neuron

Earlier we presented a model of the LGMD that was tested on mobile robots (Bermúdez et al. 2004). Here we present a further elaboration of this model that is based on the Reichardt correlation detector and that is able to work in real-world 3D environments. We quantified and successfully tested this model on a blimp-based UAV.

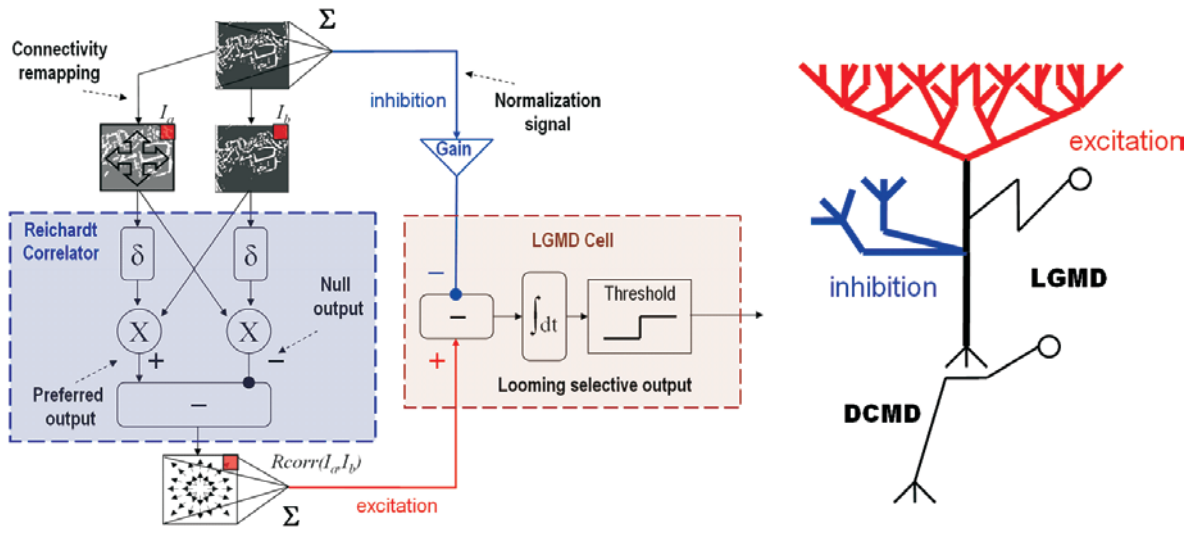

Fig. 4. LGMD model. Left panel: Implementation of the LGMD model, making use of a pre-synaptic Reichardt correlator network, where δ represents a delay, X the multiplication operation and – the subtraction operation. The LGMD integrates excitation and inhibition over time and thresholds it. Right panel: diagram of the LGMD neuron. A large excitatory pre-synaptic arborization provides the main input to the cell, and two post-synaptic inhibitory connections. The LGMD cell projects onto the, so called, Descending Contralateral Movement Detector (DCMD) that reproduces the LGMD activity 1 to 1 up to 400Hz (Rowell 1971). See text for further explanation.

Our model assumes that directional motion information of the specific motion detectors of the lamina is used *a posteriori* to detect expanding, i.e approaching stimuli. Moreover, our model proposes that the EMD responses found in the lamina are integrated by the LGMD to build up a system that is able to compute the amount of expansion from the visual input (Figure 4). The LGMD would then receive input from motion detectors and emit spikes when this integrated signal exceeds a specific threshold, i.e an integrate and fire neuron.

The neuron model is built from a capacitor C and a resistor R connected in parallel to ground on one end and driven by the current I on the other end (Koch 1999):

$$C\frac{dV(t)}{dt} + \frac{V(t)}{R} = I(t). \tag{15}$$

A switch is used to reset the membrane potential to zero after a spike. For a constant input current I the voltage is defined by:

$$\begin{aligned} V(t) &= IR \cdot (1 - \exp(-t/RC)) + V(t=0) \\ &\cdot \exp(-t/RC). \end{aligned} \tag{16}$$

The voltage at the membrane of the integrate and fire neuron will increase asymptotically to $V = IR$. While the voltage is below the firing threshold ($V < V_{Th}$) the neuron remains silent, and once V_{Th} is reached it produces an action potential (spike) and resets the membrane voltage $V(t)$ to zero. The charging time constant of the membrane potential is defined as $\tau = RC$.

Analog to the HS/VS neuron model, the Reichardt correlation is used to compute local motion at the level of pixels. A topographic remapping allows us to correlate the activity of pixels that are aligned radialy through the center of the image. This process is equivalent to the integration of the responses of the EMDs that are sensitive to radial outward motion through the center of the image (Figure 4). Then, the looming sensitivity of the LGMD model emerges from its particular connectivity with the EMD neurons. However, the more edges in the image the more activity will come out of the correlators. In our model this stimulus-dependent aspect of the neuronal responses is compensated for via post-synaptic inhibition. The sum of the pixel values of the detected edges is used as a normalizing factor via the feed-forward inhibition that renders the total input to the LGMD contrast invariant (Figure 4).

Each of the cameras mounted on the front part of the UAV feeds its own visual processing streams that converge onto a LGMD neuron. Whenever a train of spikes is produced by one of the simulated LGMD neurons, either left or right, it triggers an avoidance reaction in the opposite direction, performing a turn over of an angle that is defined by the strength of the response of the LGMD. If both right and left LGMD models are active at the same time, as can happen in corners, the avoidance reaction is a straight reverse movement. In the case of insects such as flies, they tend to land in these situations (Tammero and Dickinson 2002).

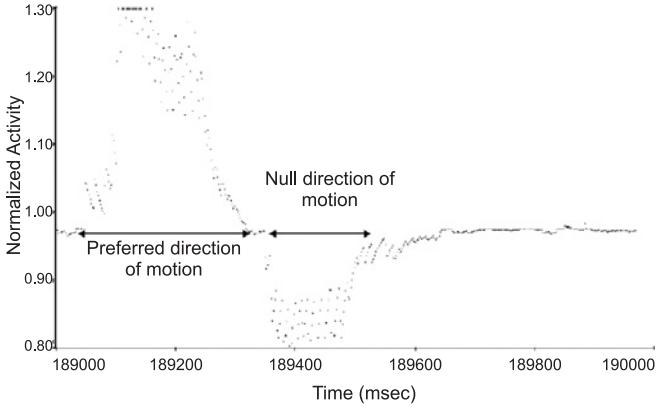

Fig. 5. Time plot of the response of a modeled wide-field motion sensitive cell (HS and VS) stimulated first in its preferred direction, then in its null direction and finally without stimulation (no motion in the visual field).

4. Results

4.1. Motion Detectors

Both the course stabilization and the collision avoidance systems of our model rely on the EMDs (equation (5)) and the wide-field HS/VS neurons that integrate these EMD responses. These neurons show a strong response to motion in their preferred direction and a reduced response to motion in their non-preferred or null direction (Egelhaaf and Borst 1993; Egelhaaf 1985). Our model indeed displays this property (Figure 5). Motion in its preferred direction produces an increase of the membrane potential while motion in the null direction has the opposite effect. Hence, the physiological signature of our EMD model is consistent with that of its biological counterpart.

4.2. Course Stabilization

Although the properties of the EMD system are rather well studied at the level of single cells and small populations, it is unclear how they collectively can contribute to course stabilization. Hence, here we evaluate their capabilities to stabilize a dirigible in the real-world. An important phenomenon observed in the dynamics of dirigibles are the effects caused by the added mass and Coriolis forces that prevent it from following a straight course. In an attempt to translate forward, a blimp acquires an angular acceleration in yaw that produces an increasing change in its heading direction over time. This is a standard engineering problem that is often solved with the integration of a gyroscope in the control system of the flying platform (Zufferey et al. 2002). Instead, our approach relies solely on vision and EMD type computations to perform this task. In order to evaluate the performance of the model, a first test is performed under ideal conditions, without wind or any other disturbance (Figure 6). The UAV is set to fly in a straight trajectory using the stabilization system to compensate for eventual drifts and perturbations. We observe that for all trials the UAV is kept on a straight trajectory.

The control experiment where the stabilization system is disabled shows that also our UAV displays a prototypical drift (Figure 6, right panel, dashed line). However, this phenomenon is totally suppressed and the UAV shows straight trajectories when the stabilization system is active. During these test flights the UAV shows a maximum off-course trajectory deviation of 15° with respect to the ideal trajectory, with a mean deviation of 7.05°. During these tests a mean velocity of 0.62 m/s is maintained.

One way to test the robustness of the stabilization system to external disturbances is by creating a controlled bias in the motor system of the robot. Our UAV is provided with independent control for altitude and translation, and therefore we can disturb the translational motor forces without modifying the altitude control. There are two bidirectional motors dedicated to forward/backward translational forces, and each of them is equipped with a four-blade propeller. In the following test, one of the propellers used for forward thrust will be replaced by a two-blade propeller. As a result this motor loses about 23% of its power, inducing a constant bias in the motor control

In the biased motor control experiment we observe a maximum off-course deviation with respect to the straight one of 10.7° (Figure 7, left panel). The mean deviation of the trajectory followed by the UAV is 7.2° with a mean forward speed of 0.23 m/s, which is practically the deviation observed without motor bias. Compared to the previous experiment the maximum off-course deviation is 5° lower. This can be explained in terms of the sensitivity threshold of the system, since higher drifts are more easily detected than very small ones. The mean deviation of the trajectory followed by the UAV is comparable between the two experiments. Hence, our model is able to completely compensate for a significant motor bias.

The last experiment assessed the efficiency of the stabilization model under extreme conditions; total absence of right propulsion. In this case the right propeller was totally removed and the UAV was forced to fly forward (Figure 7 right panel). Usually in this situation, the UAV starts turning in rightward circles in an uncontrolled manner due to the torque generated by the only remaining motor. However, the stabilization model tries to maintain always a constant heading direction (Figure 7 right panel). The result of this experiment is that after 14 seconds of free flight, the UAV was displaced just about 1 meter to the right and only slightly changed its heading direction (2.8°/s). The fact that the robot is only using the left motor has to be taken into account in order to understand the lateral displacement to the right since the UAV has no way to compensate for it. The UAV is turning right when forward commands are sent and then the stabilization system corrects for this drift.

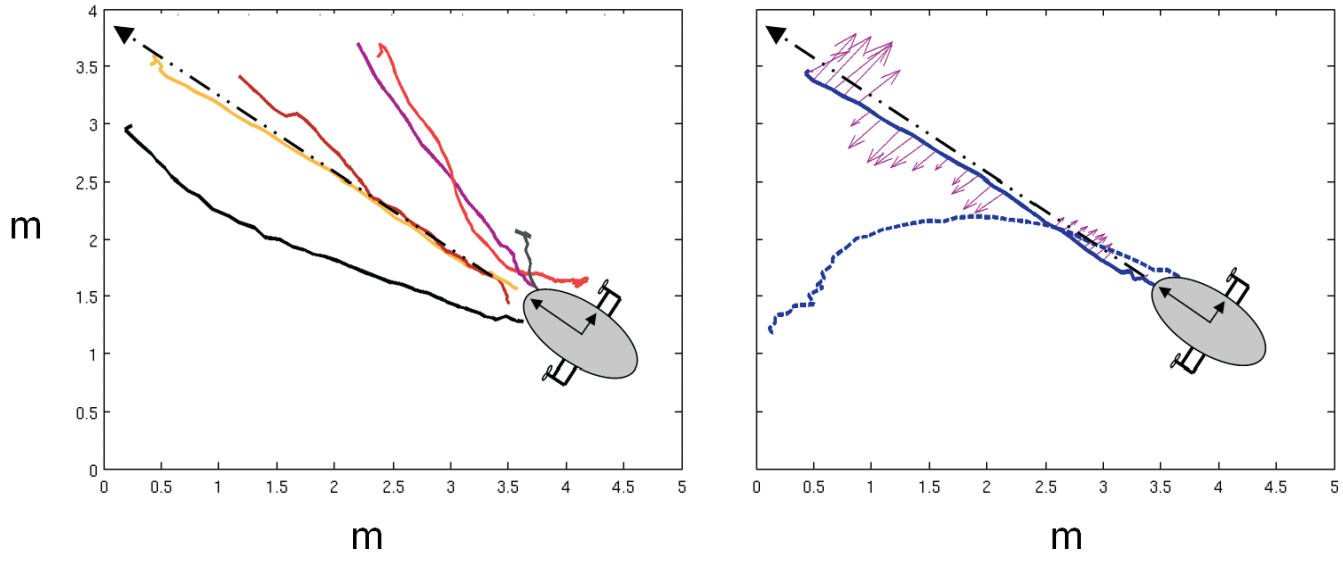

Fig. 6. Test flights traces using the stabilization model. Left panel: Six traces using the course stabilization system in our test room. Right panel: Comparison between a non-stabilized run and one with our biologically based model. The dashed line indicates the flight trajectory when the course stabilization model is disabled. The arrows on the trace represent the motor compensation forces applied to the UAV. The UAV is drawn to scale.

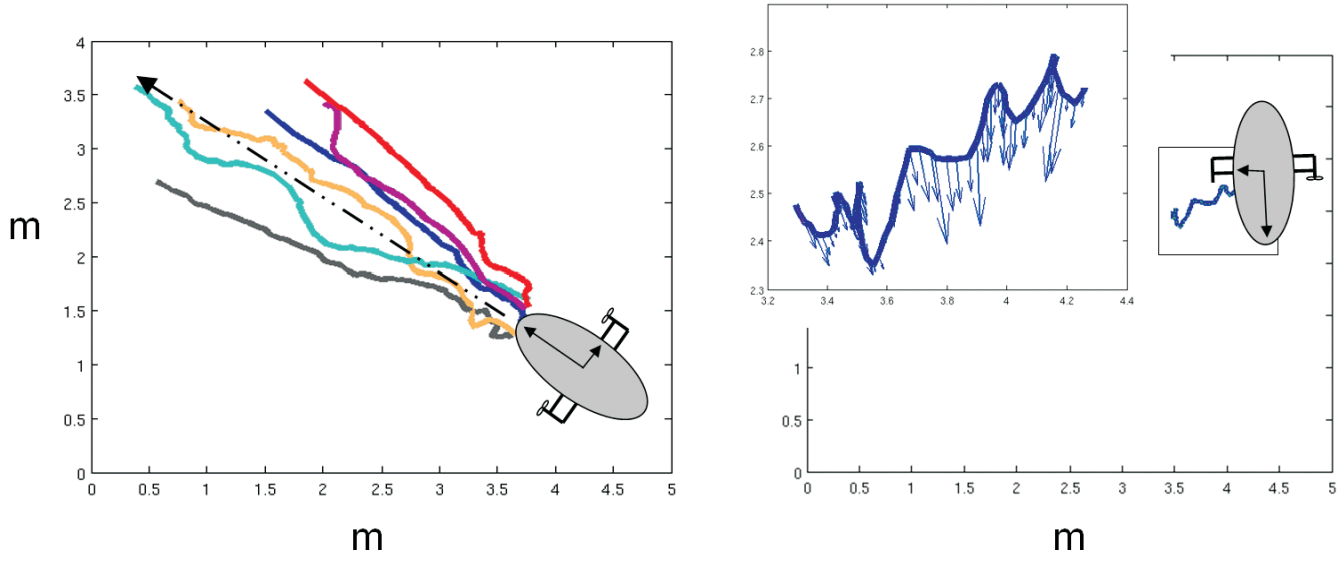

Fig. 7. Stabilization behavior with biased motor control. Left panel: Horizontal view of the trajectories of six test flights using the stabilization model for the control of an unbalanced propulsion system. Right panel: trajectory of the UAV in absence of the right propeller for a period of 14 s, resulting in a lateral displacement of about 1 m. while attempting to move forward. The direction of the arrow head indicates the heading direction of the UAV, and its length is proportional to the UAV speed. The UAV is drawn to scale.

During the duration of this experiment, the UAV has attempted to move forward 30% of the time, and it has been compensating the resultant drifts the remaining time. The resulting mean velocity is 0.08 m/s.

We compare the above three experiments by evaluating the difference of the motor actions generated (Figure 8). Under ideal conditions left and right rotations should be the same (except for the added mass and Coriolis effect), and therefore, the

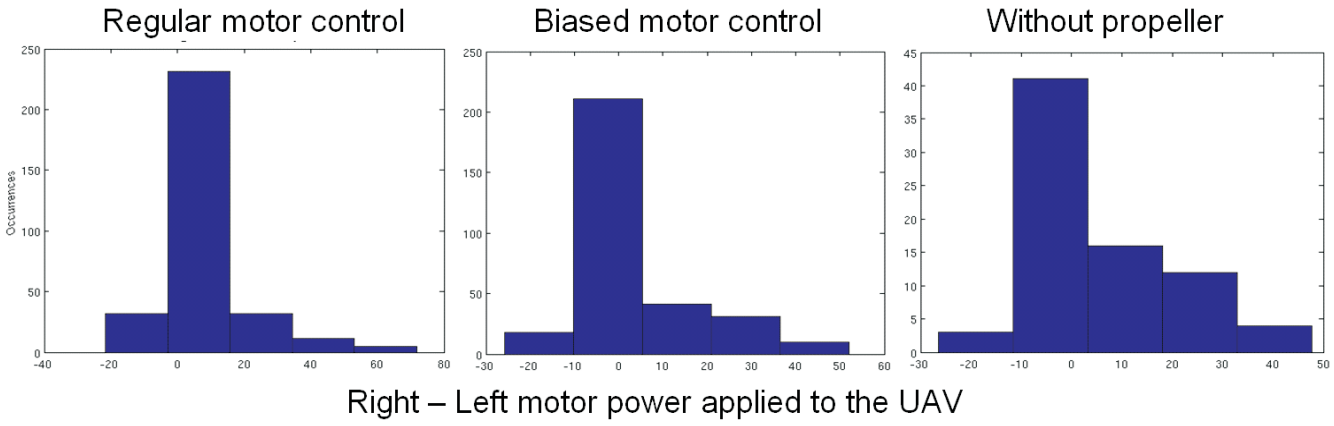

Fig. 8. Comparison of the motor actions taken in the three experiments. The histograms represent the power used for left rotation minus the one used for right rotation for three experiments: (a) unbiased motor control; (b) biased motor control and (c) removed right propeller.

histograms should be symmetrical and centered at 0. We observe that this is indeed the case for the first set of experiments (Figure 8, left panel), whereas in the case of biased motor control, the fraction of compensatory commands to the right motor increase proportional to the bias in the thrust of the right motor (66%). This effect further increases to 70% in the absence of the right propeller. Moreover, not only the compensation time increases but also the power used for the compensation actions (Figure 8). All these experiments corroborate the effectiveness and robustness of the system. Under very different conditions, our fly-based stabilization system is able to compensate drift and perturbations without compromising overall performance.

4.3. Altitude Stabilization

Our model of course stabilization can also be used for altitude control. In this case the upward and downward optic flow detected by our model is used to trigger compensation motor commands that cancel these flow patterns, i.e. keeping a constant altitude. Our analysis of the responses of the UAV shows that the motor compensation forces of the altitude control system are tightly coupled to variations of the altitude of the UAV (Figure 9 bottom panel). Thus, we can observe that the system is trying to compensate the descending tendency of the UAV with a strong upward response proportional to the vertical displacement detected with the neural model and vice versa (Figure 9 bottom panel).

All the traces obtained are found to be constrained to a narrow margin of just 0.66 m. for a journey of up to 8 s (Figure 9, top panel). The traces present a mean altitude of 1.7 m. and a standard deviation of 0.1 m. The standard deviation compared to the size of the blimp (∼ 0.6 m high) represents only about 18% of blimp height.

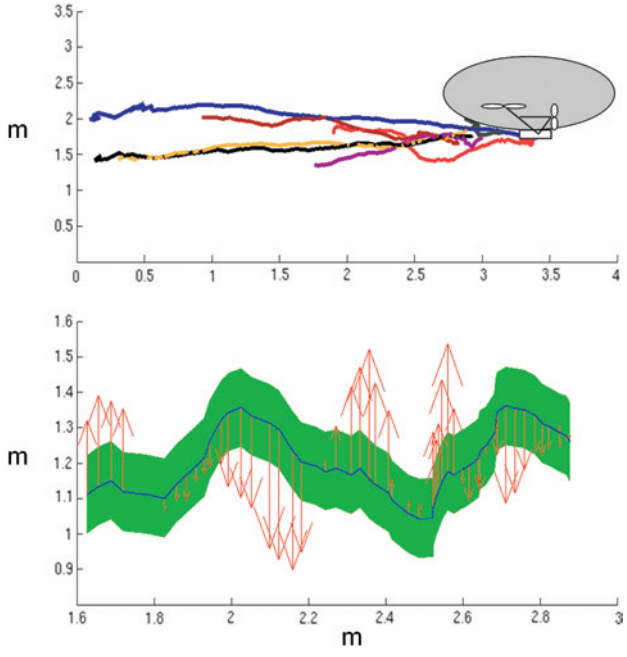

Fig. 9. Altitude control. Top panel: Lateral projection for six test traces of the UAV with non-biased motor control. Bottom panel: A selected representative trajectory with standard deviation (filled area) that shows the relationship between the behavior of the UAV and the responses of the altitude control system. The length of the arrows is proportional to the value of the motor command sent at that very moment in time. The UAV is drawn to scale.

There appears a constant delay of about one second between the instant when the blimp is displaced and the cor-

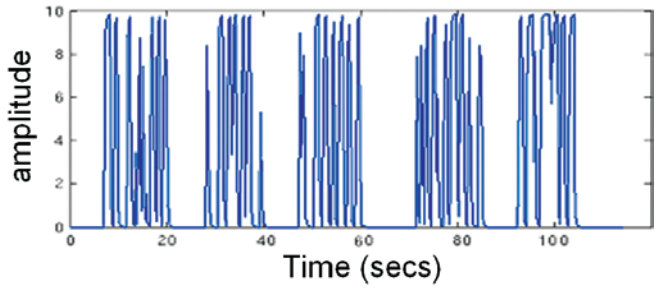

Fig. 10. Responses of the LGMD model to five consecutive approaching and receding maneuvers at 0.25 m/s. The model shows high activity when approaching whereas no activity while receding. Adapted from Bermúdez et al. (2004).

responding compensatory response (Figure 9 bottom panel). This response latency is due to the use of the Reichardt correlator model that requires integration and time delayed comparisons (Figure 3, equation (5)) and the computational cost of running this system in real time. However, the impact of this delay is negligible compared to the one caused by the large integration time required to have a reliable estimate of the optic flow. This integration time is modeled in our system by making use of high membrane persistences (equation (15)), equivalent to a low-pass filter. In addition, we are constrained by the acquisition rate of the video data which is 15 frames/s. A faster video acquisition system would reduce the latency considerably. Hence, the delays observed in our system are more due to implementation issues than to fundamental properties of the model.

4.4. Collision Avoidance

Collision avoidance in our model is based on the locust LGMD neuron. In addition to the evaluation of this model in flight tests we use an off-line method to validate its biological plausibility similar to those used in physiology (Gabbiani et al. 2002; Hatsopoulus et al. 1995). Here, in order to characterize the model responses with respect to looming stimuli, black-filled expanding and contracting squares of different sizes on a white background have been presented as visual input to the LGMD model. A distance range from 2.5 to 3.5 m is chosen for these approach maneuvers. From five to ten experiments are performed for looming speed values ranging from 0.1 m/s to 0.5 m/s.

Consistent with the properties of its biological counterpart, the responses of the model show a strong activation and a high firing rate during the approaching maneuvers whereas no activity is shown during the receding ones (Figure 10). This demonstrates the sensitivity of our model to looming, and therefore the possibility of applying it to the collision detection task.

Subsequently, 10 repetitions for a number stimulus speeds (equation (14)) were performed using the same stimuli. When we evaluate the firing rate (spikes/s) of the responses of our model LGMD neuron to different of l/v ratios (object size/object velocity) (Figure 11, left panel), an increase in the activity and a later frequency peak is observed as the stimulus speed increases. This prototypical behavior of the LGMD neurons is systematically reproduced by our model. The correlation between our model and the formal description of LGMD physiology (equation (14)) is between 0.88 and 0.94 (Figure 11, right panel). The responses of our model, however, have to be understood as an emerging property from the integration of the responses of many motion sensitive cells (EMD-like neurons) combined with a gain control signal (Figure 4) and not from the multiplication of angular speed with angular velocity *per se*. Therefore, and consistent with other EMD-based models (Harrison 2005), the explicit measurement and representation of angular speed and angular velocity are not required for the collision avoidance task.

To be successful in the collision avoidance task, the animal must not only reliably detect an imminent collision but also do it at a prudent distance. This is also crucial when dealing with fast moving vehicles, vehicles with slow reaction times or when the inertial forces play an important role, as in the case of dirigibles and underwater vehicles. Hence, we have assessed this relationship between distance and detection for our LGMD model (Figure 12). Our analysis shows a later response for high speeds, being in the worst case at a distance around 1.75 m. In addition, the peak in firing frequency always occurs before the collision happens, largely independent of the approaching speed. These results show that the responses of our model LGMD are consistent with those of its biological counterpart and that it can provide information that can be used for obstacle avoidance.

To measure the performance of the collision avoidance model we counted the number of successfully detected collisions, false detections and missed collisions using a ground robot in an arena delimited by randomly textured walls. We observed that 89% of the collisions are successfully detected and 7% are false positives and 4% missed collisions.

4.5. Behavior

We evaluate the overall performance of our biologically based control model in free flight experiments where the UAV is controlled by the combined course stabilization, altitude control and collision avoidance neural models. This experiment consists of a four minutes flight in our $5 \times 4 \times 4.5$ m test room. We observe that during this period the UAV is able to negotiate this environment with a minimal number of collisions, showing continuous flight without getting trapped in corners. The LGMD model shows obstacle detection at a mean distance of 1.7 m. from the wall within a range of 1 to 2.7. The largest

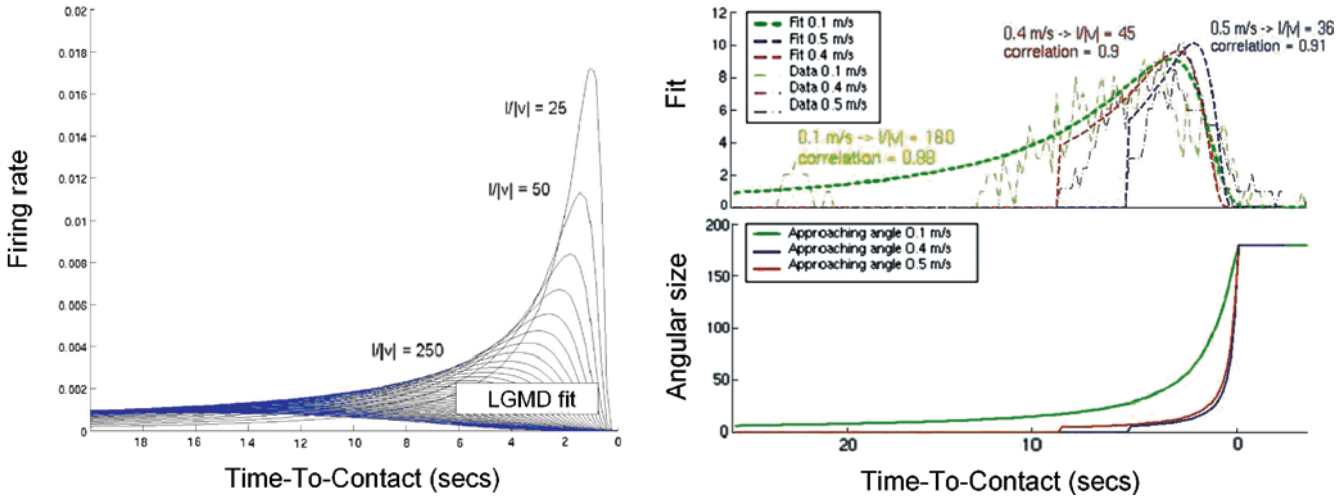

Fig. 11. Response characteristics of the model LGMD. Left panel: Theoretical evolution of the LGMD responses according to equation (14) for a range of looming speeds, where the ratio $l/|v|$ represents the ratio between object size and speed. Right panel top: Measured evolution of our model responses with the $l/|v|$ ratio. The raw data of our model is fitted using equation (14). Right panel bottom: Evolution of the angular size of the looming object over time. Ten approaching maneuvers have been performed for every speed (0.1, 0.4 and 0.5 m/s).

distance in the test room is about 6.5 m (Figure 13). This mean obstacle detection distance is calculated using the first LGMD model spike as the position at which the system detects the collision. Avoidance maneuvers are performed with a mean time of 3.9 s. In order to trigger an avoidance reaction the LGMD model response is integrated for some time, and when this integrated response exceeds a certain threshold a collision avoidance maneuver is triggered. This integration over time avoids having false positive detections while allowing the UAV to get closer to the walls, and therefore explore a bigger area. This explains that a collision can be detected at 2 m from the wall but a reaction is not triggered until the UAV is close to the wall (Figure 13). Hence, at this point a trade-off between the speed of the UAV and its collision detection appears. The higher the flight speed, the faster the rate of looming of stimuli in front of the UAV, although less time is available to avoid it. In addition, we observe that the flight trajectories between the different points of rotation, i.e. avoidance, are practically straight due to the drift compensation mechanisms or our model. The altitude standard deviation of the blimp during this experiment was 0.16 m.

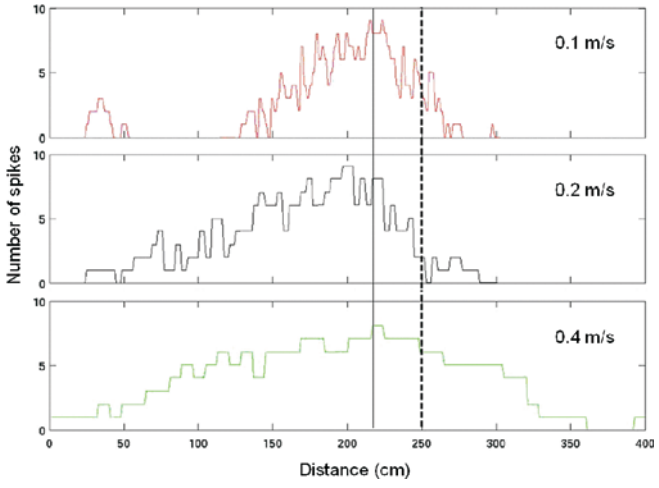

Fig. 12. Firing rate versus distance of the stimulus to the LGMD model for a constant stimulus size and three different approaching speeds (0.1, 0.2 and 0.4 m/s). Collision distance and the peak firing rates are marked with a dashed line and solid line respectively. Each trace corresponds to an average of 10 approaching maneuvers.

5. Discussion and Conclusions

We have presented a model of flight control, including course stabilization, altitude control and obstacle avoidance, based on our current understanding of the opto-motor systems implemented in the brains of flying insects. These experiments demonstrate that the underlying principles of insect visual navigation can be generalized to UAVs, and that autonomous flight can be achieved by the combination of simple reactive systems. The simplicity of these three insect-based reactive systems (course stabilization, altitude control and collision avoidance) is reflected in a low computational cost, no use of

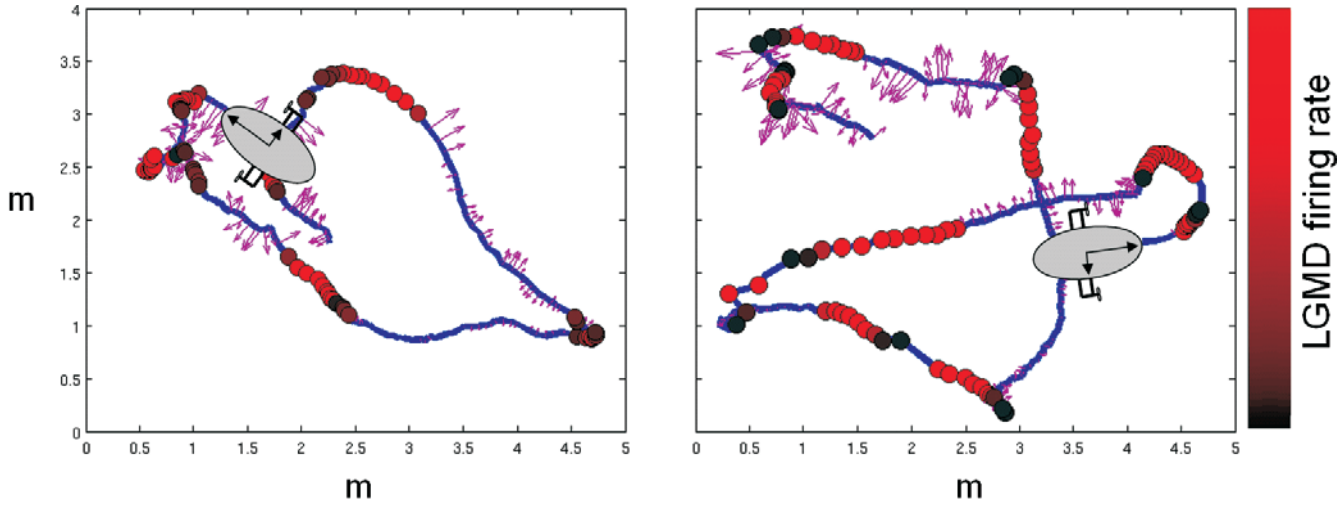

Fig. 13. Free flight traces of the UAV in our test room. Example of a one minute trace of the UAV flying autonomously controlled by our neural model. The trace represents the position of the UAV, the arrows are the compensatory course stabilization forces generated by the model, and the intensity coded dots represent the activity from the LGMD collision detection model. The dots are only present when the LGMD activity > 0, the intensity is proportional to the firing rate.

additional memory or any training period. Moreover, the property of extracting optic flow from the image via correlations makes this system very robust in terms of its independence on the textures of the surfaces it encounters as long as any visual cue is present (Hengstenberg 1982).

Our experiments demonstrated the performance of the different model components separately as well as in combination applied to a UAV under a range of conditions, including the absence of one propeller. As the conditions become worse and the UAV does not respond as was expected (biased motor control), the percentage of time invested in compensating course drifts increases, going from 60% of the time under ideal conditions up to 70%. The increase of compensatory motor commands results in a considerable decrease in the speed of the UAV, this being 0.62 m/s for unbiased motor control and 0.23 m/s for biased control. However, the insect-based models adapt to each situation and are able to generate a straight course with a mean off-course deviation of no more than about 7°. Furthermore, the altitude control system allows us to keep a constant altitude with a standard deviation value of only 0.1 m, i.e. about 20% of the size of the device. However, the motion sensitive cells we model are specifically tuned to respond maximally at a given speed (equation (10)), suggesting that a combination of EMDs tuned to different speeds would also provide a speed invariant response.

The presented LGMD collision avoidance model has been characterized for a range of speeds and is able to reliably predict an imminent collision (∼1.7 m distance). We have shown that it can be successfully applied to flying robots with speeds of up to 1 m/s. This model allows us to detect collisions at a prudent distance from the obstacle, being a good candidate to be applied in relatively fast robots or where the environmental conditions do not permit a fast response (underwater or aerial vehicles).

Other behaviorally similar collision avoidance models have recently been proposed to explain the behavior of the saccades of the fruit fly Drosophila Melanogaster, which are triggered in order to avoid collisions (Tammero and Dickinson 2002), but these have so far never been implemented. A very similar approach to the one proposed here was implemented on an aVLSI chip and has been evaluated using a terrestrial robot (Harrison 2005).

The correlation values obtained support the similarity between our LGMD model and its biological counterpart. However, the specific connectivity of the LGMD is not yet well defined, and it is not clear whether motion sensitive neurons could provide the main excitatory input to this neuron. The basic structure of the LGMD is known since the 1970s (Rowell 1971), but so far there is no evidence of what the connectivity with its pre-synaptic layers is. Therefore we don't know yet what information is used and processed by the LGMD, and where its sensitivity to looming exactly comes from. Hence, there are still a number of issues to be studied, like the particular non-linear properties of the LGMD found that was recently reported (Gabbiani et al. 2002; Hatsopoulus et al. 1995), its concrete pre-synaptic connectivity and whether the EMD type of neuron is a valid model for the neurons previous to the LGMD in the Medulla layer. Our model leads to quantitatively and qualitatively similar results to the ones obtained by experiments on the locust (Hatsopoulus et al. 1995; Gabbiani 1999; Gabbiani et al. 2001; Gabbiani et al. 2002), suggesting that both could be based on the same principles. Our model

is unique in the sense that we have shown that the principles underlying the LGMD detection system can both match the physiology of this system and reliably control a flying vehicle. In addition, in our approach we present realistic task specific insect-based models that allow a blimp based UAV to perform successful course stabilization, altitude control and obstacle avoidance.

Many different UAV systems are in use and small helicopter-based UAVs might be more appealing than blimp-based ones, but these do require the experimenter to deal with a number of additional handicaps. Model-sized helicopters have a short flight time and the time constants describing their dynamics are very short. Therefore, due to the difficult dynamics, these devices are unstable and tremendously demanding on the flight control side. This means that in order to solve basic navigation problems one is obliged to resort to inertial sensors (Skafidas 2002; Musial et al. 2000). The fact that some platforms require the use of specific sensors for basic navigation tasks implies that methods or systems must be developed to process their data and perform the actual control task. A dirigible type platform is a good compromise between the complexity of a helicopter based UAV and the oversimplification that accompanies the use of ground based robots. Some attempts to control blimp-based UAVs without specialized sensors use optimization approaches such as evolutionary algorithms and hence require a considerable training period to adapt to the environment (Zufferey et al. 2002). In Iida (2001), an EMD-based system used for stabilization is also used for obstacle avoidance, trying to compensate the asymmetries of the optical flow when an agent is getting close to a wall. Therefore, it is avoiding collisions since it tries to maintain the UAV flying at the same "apparent distance" from the reference walls. The immediate engineering or biological relevance of this approach, however, is not obvious.

Our results show for the first time that the neuronal principles of flight control found in insects can be successfully generalized to the control of a flying robot. This generalization is robust and also computationally efficient. Our flight control system is part of a larger model that also includes mechanisms for chemical search and localization based on the moth pheromone communication system (Pykk et al. 2006). This biologically based flight control system will be used to control a fleet of autonomous UAVs with chemo-sensing capabilities for environmental monitoring. As such our approach shows the synergy that can be found between the life sciences and engineering where we use robotic technology to understand the brain while using the acquired insights to construct novel real-world technologies.

Acknowledgements

The authors would like to thank Ulysses Bernardet for help with iqr421 (Bernardet et al. 2002). This work is supported by the AMOTH project, and was supported by the EU. This research is supported by the European Community and BBW (Grant "A Fleet of Artificial Chemo sensing Moths for Distributed Environmental Monitoring (AMOTH)" to PFMJV, funded under the IST Future and Emerging Technologies Programme (IST-2001-33066, project website http://www.amoth.org/).

References

Bermúdez, i. Badia, S., and Verschure, P. F. M. J. (2004). A collision avoidance model based on the Lobula Giant Movement Detector (LGMD) neuron of the locust. In *Proceedings of International Joint Conference on Neural Networks* (IJCNN'04).

Bernardet, U, Blanchard, M., and Verschure, P. F. M. J. (2002). IQR: a distributed system for real-time real-world neuronal simulation. *Neurocomputing*, 44–46: 1043–1048.

Blanchard, M. and Verschure, P. F. M. J. (1999). Using a mobile robot to study locust collision avoidance responses. *International Journal of Neural Systems*, **9**(5): 405–410.

Blanchard, M., Rind, F. C., and Verschure, P. F. M. J. (2001). How accurate need sensory coding be for behaviour? Experiments using a mobile robot. *Neurocomputing*, **38–40**: 1113–1119.

Braitenberg, V. (1967). Patterns of projections in the visual system of the fly. I. Retina-Lamina projections. *Experimental Brain Research*, **3**: 227–298.

Douglas, J. K. and Strausfeld, N. J. (1996). Visual motion-detection circuits in flies: parallel direction- and non-direction-sensitive pathways between the medulla and lobula plate. *The Journal of Neuroscience*, **16**(15): 4551–4562.

Dudley, R. (2000). The biomechanics of insect flight: form, function, evolution. *Annals of the Entomological Society of America*, **93**(5): 1195–1196.

Egelhaaf, M. and Borst, A. (1993). Motion computation and visual orientation in flies. *Comput. Biochem. Physiol.* **104A**: 659–673.

Egelhaaf, M. (1985). On the neural basis of figure ground discrimination by relative motion in the visual system of the fly. I. Behavioral constraints imposed on the neuronal network and the role of optomotor system. *Biol. Cybern.* **52**: 123–140.

Kelly, F. C. (1950). *The Wright Brothers: A Biography Authorized by Orville Wright*. Farrar, Straus and Young, New York.

Franceschini, N., Pichon, J. M., and Blanes, C. (1992). From insect vision to robot vision. *Phil. Trans. R. Soc. B*, **337**: 283–294.

Gabbiani, F., Krapp, H. G., and Laurent, G. (1999). Computation of object approach by a wide-field, motion-sensitive neuron. *J Neurosci*, **19**(3): 1122–41.

Gabbiani, F., Krapp, H. G., Koch, C., and Laurent, G. (2002). Multiplicative computation in a visual neuron sensitive to looming. *Nature*, **420**: 320–324.

Gabbiani, F., Mo, C., and Laurent, G. (2001). Invariance of angular threshold computation in a wide-field looming-sensitive neuron. *The Journal of Neuroscience*, **21**(1): 314–329.

Gonzalez, R. and Woods, R. (1992). *Digital Image Processing*, Addison-Wesley, p 442.

Hafner, V. V., Kunz, H., and Pfeifer, R. (2002). An investigation into obstacle avoidance as an 'emergent' behaviour from two different perspectives. In *Proceedings of the EPSRC/BBSRC International Workshop on Biologically-inspired Robotics*. The legacy of W. Grey Walter, pp. 166–173.

Hafner, V. V. and Salomon, R. (2002). Evolving neural controllers for visual navigation. In *Proceedings of the 2002 Congress on Evolutionary Computation*.

Harrison, R. R. (2005). A biologically-inspired analog IC for visual collision detection. *IEEE Transactions on Circuits and Systems-I*, **52**: 2308–2318.

Hatsopoulus, N., Gabbiani, F., and Laurent, G. (1995). Elementary computation of object approach by a wide-field visual neuron. *Science*, **270**: 1000–1003.

Hengstenberg, R. (1982). Common visual response properties of giant vertical cells in the lobula plate of the blowfly Calliphora. *Journal of Comparative Physiology*, **149**: 179–193.

Higgins, C. M., Douglass, J. K., and Strausfeld N. J. (2004). The computational basis of an identified neuronal circuit for elementary motion detection in dipterous insects. *Vis. Neurosci.*, **21**(4): 567–86.

Ichikawa, M., Yamada, H., and Takeuchi, J. (2001). A flying robot controlled by a biologically inspired vision system. In *Proceedings of the 8th International Conference on Neural Information Processing (ICONIP-2001)*, Shanghai, China.

Iida, F. (2001). Goal-directed navigation of an autonomous flying robot using biologically inspired cheap vision. In *Proceedings of the 32nd ISR (International Symposium on Robotics)*, pp. 19–21.

Kern, R., Lutterklas, M., Petereit, C., Lindemann, J. P., and Egelhaaf, M. (2001). Neural processing of behaviourally generated optic flow: Experiments and model simulations. *Network: Computations in Neural systems*, **12**(3): 351–369.

Koch, C. (1999). *Biophysics of Computation: Information Processing in Single Neurons*. Oxford University Press, New York.

Levine, M. D. (1985). *Vision in Man and Machine*, McGraw-Hill Book Company.

Martin, N. and Franceschini, N. (1994). Obstacle avoidance and speed control in a mobile vehicle equipped with a compound eye. In *Intelligent Vehicles* (ed. EI. Masaki), pp. 381–386, MIT Press, Cambridge, MA.

Marden, J. H. (2005). Review: scaling of maximum net force output by motors used for locomotion. *The Journal of Experimental Biology*, **208**: 1653–1664.

Musial, M., Brandenburg, U. W., and Hommel G. (2000). MARVIN – Technische Universität Berlin's flying robot for the IARC Millennial Event. http://pdv.cs.tu-berlin.de/MARVIN/. In *Proceedings of the Symposium of the Association for Unmanned Vehicle Systems 2000*, Orlando, FL.

Netter, T. and Franceschini, N. (2002). A robotic aircraft that follows terrain using a neuromorphic eye. In *Proceedings of IEEE/RSJ IROS2002*, paper 593.

Posey, K. L., Jones, L. B., Cerda, R., Bajaj, M., Huynh, T., Hardin, P. E., and Hardin S. H. (2001). Survey of transcripts in the adult Drosophila brain. *Genome Biol*. 2: RESEARCH0008.

Pyk, P., Bermúdez i Badia, S., Bernardet, U., Knuesel, P., Carlsson, M., Gu, J., Chanie, E., Hansson, B. S., Pearce, T. C., and Verschure, P. F. M. J. (2006). An artificial moth: Chemical source localization using a robot based neuronal model of moth optomotor anemotactic search. *Autonomous Robots*, **20**(3):197–213.

Ready, D. F., Hanson, T. E., and Benzer, S. (1976). Development of the Drosophila retina, a neurocrystalline lattice. *Development Biology,* **53**(2): 217–40.

Reichardt, W. (1961). Autocorrelation, A principle for the evaluation of sensory information by the central nervous system. In: Sensory communication, Rosenblith WA, pp 303–317. New York: MIT Press-Willey.

Rowell, C. H. (1971). The orthopteran descending movement detector (dmd) neurones: a characterisation and review. *Zeitschrift für vergleichende Physiologie*, **73**: 167–194.

Saripalli, S., Montgomery, J. F., and Sukhatme, G. S. (2003). Visually-guided landing of Unmanned Aerial Vehicle. http://Citeseer.nj.nec.com/saripalli03visuallyguided.html.

Schilstra, C. and van Hateren, J. H. (1999). Blowfly flight and optic flow: I. Thorax kinematics and flight dynamics. *The Journal of Experimental Biology*, **202**: 1481–1490.

Skafidas, A. (2002). *Micro-controller Systems for a UAV, Auto Piloting and Camera Trigger System*, Albanova University Centre (BSC Thesis), Physics Department. ISSN 0280-316 X. More detail required

Srinivasan, M. V., Zhang, S. W., Lehre, M. R., and Collett, T. S. (1996). Honeybee navigation en route to the goal: visual flight control and odometry. *J. Exp. Biol*, **199**: 237–244.

Strausfeld, N. J. (1976). *Atlas of an Insect Brain*, Springer-Verlag, New York.

Tammero, L. F. and Dickinson, M. H. (2002). The influence of visual landscape on the flight behavior of fruit fly Drosophila Melanogaster. *The Journal of Experimental Biology*, **205**: 327–343.

Zufferey, J. C., Floreano, D., van Leguen, M., and Merenda, T. (2002). Evolving vision-based flying robots. In *Proceedings of the 2nd International Workshop on Biologically Motivated Computer Vision*, LNCS 2525, Springer-Verlag, Berlin, pp. 592–600.